Articles

Purification and Characterization of the Fe^{II}- and α-Ketoglutarate-Dependent Xanthine Hydroxylase from *Aspergillus nidulans*†

Gabriela M. Montero-Morán,[‡,§] Meng Li,[§,||] Erika Rendòn-Huerta,[⊥] Fabrice Jourdan,[@] David J. Lowe,[@] Andrew W. Stumpff-Kane,[#] Michael Feig,[||,#] Claudio Scazzocchio,[‡,+] and Robert P. Hausinger*[,#,∞]

Institut de Génétique et de Microbiologie, Université Paris-Sud, Bâtiment 409, UMR 8621 CNRS, 91405 Orsay Cedex, France, Department of Chemistry, Michigan State University, East Lansing, Michigan 48824-1322, Departamento de Bioquimica, Facultad de Medicina, Universidad Nacional Autonoma de Mexico, Mexico City, DF, Mexico, Department of Biological Chemistry, John Innes Centre, Colney Lane, Norwich NR4 7UH, U.K., Department of Biochemistry and Molecular Biology, Michigan State University, East Lansing, Michigan 48824-1319, Institut Universitaire de France, Paris, France, and Department of Microbiology and Molecular Genetics, Michigan State University, East Lansing, Michigan 48824-4320

Received January 12, 2007; Revised Manuscript Received February 20, 2007

ABSTRACT: His_6-tagged xanthine/α-ketoglutarate (αKG) dioxygenase (XanA) of *Aspergillus nidulans* was purified from both the fungal mycelium and recombinant *Escherichia coli* cells, and the properties of the two forms of the protein were compared. Evidence was obtained for both N- and O-linked glycosylation on the fungus-derived XanA, which aggregates into an apparent dodecamer, while bacterium-derived XanA is free of glycosylation and behaves as a monomer. Immunological methods identify phosphothreonine in both forms of XanA, with phosphoserine also detected in the bacterium-derived protein. Mass spectrometric analysis confirms glycosylation and phosphorylation of the fungus-derived sample, which also undergoes extensive truncation at its amino terminus. Despite the major differences in the properties of these proteins, their kinetic parameters are similar (k_{cat} = 30−70 s^{-1}, K_m of αKG = 31−50 μM, K_m of xanthine ∼ 45 μM, and pH optima at 7.0−7.4). The enzyme exhibits no significant isotope effect when [8-^{2}H]xanthine is used; however, it demonstrates a 2-fold solvent deuterium isotope effect. Cu^{II} and Zn^{II} potently inhibit the Fe^{II}-specific enzyme, whereas Co^{II}, Mn^{II}, and Ni^{II} are weaker inhibitors. NaCl decreases the k_{cat} and increases the K_m of both αKG and xanthine. The αKG cosubstrate can be substituted with α-ketoadipate (9-fold decrease in k_{cat} and 5-fold increase in the K_m compared to those of the normal α-keto acid), while the αKG analogue *N*-oxalylglycine is a competitive inhibitor (K_i = 0.12 μM). No alternative purines effectively substitute for xanthine as a substrate, and only one purine analogue (6,8-dihydroxypurine) results in significant inhibition. Quenching of the endogenous fluorescence of the two enzyme forms by xanthine, αKG, and DHP was used to characterize their binding properties. A XanA homology model was generated on the basis of the structure of the related enzyme TauD (PDB entry 1OS7) and provided insights into the sites of posttranslational modification and substrate binding. These studies represent the first biochemical characterization of purified xanthine/αKG dioxygenase.

Most organisms that metabolize xanthine possess a molybdopterin cofactor-containing enzyme that hydroxylates the substrate to form uric acid while transferring electrons to NAD (xanthine dehydrogenase) or oxygen (xanthine oxidase) (*1*). These enzymes, here called xanthine hydroxylases, are conserved throughout living organisms, including archaea, bacteria, fungi, plants, and metazoans.

In 2005, a novel mechanism for xanthine metabolism was discovered in certain fungi (*2*). This finding arose out of the observation that all mutants of *Aspergillus nidulans* defective in xanthine dehydrogenase (i.e., with mutations affecting the structural *hxA* gene, the *cnx* genes for Moco synthesis, or the *hxB* gene for sulfuration of Moco) retained the ability to grow on xanthine as a sole nitrogen source (*2*, *3*). A mutation

† These studies were supported by the National Institutes of Health (Grant GM063584 to R.P.H.), NSF CAREER Grant 0447799 (to M.F.), Université Paris-Sud (including a postdoctoral fellowship to G.M.M.-M.), CNRS and the Institut Universitaire de France (to C.S.), and EU Contract HPRN-CT-1999-084 (XONET to D.J.L. and C.S.).

* To whom correspondence should be addressed. Telephone: (517) 355-6463, ext. 1610. Fax: (517) 353-8957. E-mail: hausinge@msu.edu.

‡ Université Paris-Sud.

§ These authors contributed equally to this work.

|| Department of Chemistry, Michigan State University.

⊥ Universidad Nacional Autonoma de Mexico.

@ John Innes Centre.

Department of Biochemistry and Molecular Biology, Michigan State University.

+ Institut Universitaire de France.

∞ Department of Microbiology and Molecular Genetics, Michigan State University.

10.1021/bi700065h CCC: $37.00 © 2007 American Chemical Society
Published on Web 04/13/2007

Scheme 1

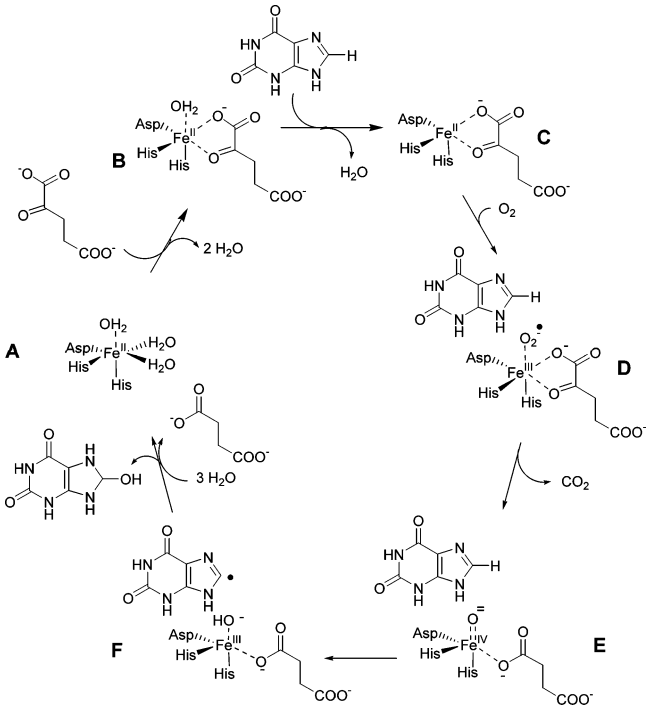

affecting this alternative process was identified, and the cognate *xanA* gene was localized to chromosome VIII (*4*). Subsequently, the *xanA* gene and its homologues from *Schizosaccharomyces pombe* and *Neurospora crassa* were cloned, and further homologues were identified in several other fungi (but not outside the fungal kingdom). The *xanA* gene of *A. nidulans* is transcriptionally coregulated with all other genes of the purine utilization pathway, including *hxA*, with its transcription depending on the same DNA binding factors, and this provides further evidence that its physiological role is xanthine oxidation (*5*). The XanA sequence shows some similarity with the taurine/α-ketoglutarate (αKG)[1] dioxygenase (TauD) group of Fe^{II}- and αKG-dependent dioxygenases (*2*), including a clear conservation of the Fe^{II}- and αKG-binding sites. This homology suggested that the alternative xanthine oxidation mechanism present in some fungi might utilize an Fe^{II}-dependent xanthine/αKG dioxygenase. Such activity was demonstrated in both crude and partially purified extracts of fungal mycelia of strains that expressed the *xanA* gene (*2*). On the basis of the previously described mechanism for Fe^{II}/αKG hydroxylases (*6*), XanA is proposed to catalyze the series of reactions (αKG binding, xanthine binding, O_2 binding, αKG decomposition and O−O cleavage to yield an Fe^{IV}−oxo species, hydrogen atom abstraction, and hydroxyl radical rebound) depicted in Scheme 1.

The wide range of Fe^{II}/αKG hydroxylases utilize a diverse array of primary substrates (reviewed in ref *6*); however, XanA is the first described enzyme of this group to hydroxylate a free purine base. In the fungal kingdom, this enzyme coexists with the classical xanthine hydroxylase; i.e., some fungi possess both xanthine hydroxylase and xanthine/αKG dioxygenase, while others possess only one or the other. Notably, yeasts as evolutionarily distant as *S. pombe* and *Kluveromyces lactis* are able to metabolize xanthine through the activity of a XanA homologue (*2*). They lack a classical xanthine dehydrogenase, and they are incapable of synthesizing Moco, which is universally present in the classical xanthine hydroxylases. The discovery of the novel Fe^{II}- and αKG-dependent XanA enzyme poses both evolutionary and mechanistic problems. Is the xanthine-binding site of the newly identified enzyme at all similar to that of the classical xanthine hydroxylases (*7*, *8*) or to the recently described xanthine transporters (*9*, *10*)? Is the mechanism of hydroxylation similar to that described for TauD (*11*, *12*)? What are the evolutionary advantages and disadvantages of possessing the Moco-containing and Fe^{II}- and αKG-dependent enzymes?

As a first step toward answering these questions, we have purified His_6-tagged versions of XanA from its natural host, *A. nidulans*, and from *Escherichia coli*. We show that the protein differs in quaternary structure and in the identity of posttranslational modifications depending on whether it is derived from the fungal or bacterial host. In addition, we demonstrate that the fungus-derived protein is truncated at its amino terminus. We confirm that the enzyme is an Fe^{II}/αKG dioxygenase and show that the two forms of the protein exhibit similar pH dependence and kinetic parameters. We show that the enzyme exhibits a solvent isotope effect, but not a substrate isotope effect. In addition, we define the effects of different divalent metal ions, salt, and several αKG and xanthine analogues, including identification of alternate substrates and inhibitors. We use the endogenous fluorescence of the enzyme to monitor binding of αKG, xanthine, and a purine inhibitor and deduce their dissociation constants. Finally, we generate a homology model of XanA and use it to provide insights into the likely sites of posttranslational modification and substrate binding. These studies present the first biochemical analyses of purified Fe^{II}-dependent xanthine/αKG dioxygenase.

EXPERIMENTAL PROCEDURES

Cloning for Overproduction of His_6-Tagged XanA in A. nidulans and E. coli, Growth of Mycelia and Bacterial Cells, and Purification of XanA from Each Source. The details of these procedures are provided in the Supporting Information. Enzyme samples were stored in buffer containing EDTA and/or imidazole to ensure the presence of the apoprotein; these conditions minimize the aberrant metal-dependent side reactions known to damage other related enzymes (*13*−*16*).

Protein Analytical Methods. Routine determinations of protein concentration were carried out by the method of Bradford (*17*) with bovine serum albumin used as the standard. Qualitative measurement of protein overexpression and assessment of protein purity made use of sodium dodecyl sulfate−polyacrylamide gel electrophoresis (SDS−PAGE) (*18*), with stacking and running gels containing 5 and 12% acrylamide. Standard proteins used for comparison included phosphorylase *b* (M_r = 97 400), bovine serum albumin (M_r = 66 200), ovalbumin (M_r = 45 000), carbonic anhydrase (M_r = 31 000), trypsin inhibitor (M_r = 21 500), and lysozyme (M_r = 14 400) (Bio-Rad Laboratories) or phosphorylase *b* (M_r = 97 400), bovine serum albumin (M_r = 66 200),

[1] Abbreviations: αKG, α-ketoglutarate; DHP, dihydroxypurine; Moco, molybdopterin cofactor; NOG, *N*-oxalylglycine; NTA, nitrilotriacetic acid; PIXE, particle-induced X-ray emission; PNGase F, *N*-glycosidase F; SDS−PAGE, sodium dodecyl sulfate−polyacrylamide gel electrophoresis; TauD, taurine/αKG dioxygenase.

ovalbumin ($M_r = 45\,000$), carbonic anhydrase ($M_r = 30\,000$), trypsin inhibitor ($M_r = 20\,100$), and α-lactalbumin ($M_r = 14\,400$) (GE Healthcare Life Sciences). The native size of XanA isolated from each host source was estimated by gel filtration chromatography using a Protein-pak Diol(OH) 10 μm column [Waters, 0.5 or 1 min/mL at room temperature in 100 mM Tris buffer (pH 7.5) containing 300 mM NaCl], a Superose 6 HR 10/30 GL column [Pharmacia, 1 mL/min in 50 mM MOPS (pH 6.8) containing 0.15 M NaCl], or a Superdex 200 HR 10/30 column [Pharmacia, 0.4 mL/min in 50 mM MOPS (pH 6.8) with 0.15 M NaCl]. The calibration proteins were thyroglobulin ($M_r = 670\,000$), γ-globulin ($M_r = 158\,000$), ovalbumin ($M_r = 44\,000$), myoglobin ($M_r = 17\,000$), and vitamin B_{12} ($M_r = 1350$) (Bio-Rad) along with ferritin ($M_r = 440\,000$), catalase ($M_r = 232\,000$), aldolase ($M_r = 158\,000$), and yeast alcohol dehydrogenase ($M_r = 150\,000$). A Beckman LF 3000 N-terminal Edman sequencer (Beckman System Gold) was used in attempts to examine the N-terminal amino acid residues of the XanA enzyme isolated from both *E. coli* and *A. nidulans*.

Analysis of Posttranslational Modifications. The XanA protein samples were tested for the presence of glycoconjugates by using the DIG Glycan Detection kit (Roche). As described above, 5 μg of each protein sample was separated via 12% SDS−PAGE, transferred to nitrocellulose, and reacted with the enzyme immunoassay reagents. In addition, XanA samples were enzymatically deglycosylated by using *N*-glycosidase F (PNGase F), an enzyme that can remove all types of N-linked oligosaccharides from glycoproteins (*19*). The enzymatic treatment was carried out with both the native and denatured XanA samples (20 μg). Denaturation was carried out in buffer containing 0.5% SDS and 0.4% dithiothreitol at 95 °C for 5 min (final volume, 25 μL) and then treated with 3 units of PNGase F in buffer [50 mM sodium phosphate (pH 7.5) supplemented with 1% NP-40] at 37 °C for 2 h (final volume, 33 μL). The reactions were stopped by transferring the samples onto ice, followed by 5 min at 95 °C. After digestion, samples were analyzed by SDS−PAGE and compared to protein size markers obtained from Fermentas Life Sciences.

To test for the presence and identify the types of phosphorylation in each of the XanA samples, the proteins (5 μg) were separated by 12% SDS−PAGE and transferred to 0.45 μm nitrocellulose (Micron Separation) at 120 mA for 1 h by using a semidry transfer cell (Bio-Rad). Nonspecific binding was blocked by incubating the samples with 5% milk protein for 1 h before incubating them with rabbit polyclonal anti-phosphoserine, rabbit polyclonal anti-phosphothreonine, or mouse monoclonal anti-phosphotyrosine antibodies (ZYMED, South San Francisco, CA) at 1 μg/mL. A horseradish peroxidase-labeled secondary antibody was then used in conjunction with an ECL Western blotting detection system (Amersham Biosciences, Little Chalfont Bucks, U.K.). The labeled immunoblot was placed against reflection autoradiography film (Kodak X-Omat XK-1) and developed for 1 s. Kaleidoscope protein size markers were obtained from Bio-Rad Laboratories.

Mass Spectrometry. Mass spectrometry analyses were performed using a Waters (Milford, MA) LCT Premier mass spectrometer coupled to a Shimadzu (Columbia, MD) LC-20AD HPLC system and SIL-5000 autosampler. Samples were analyzed using electrospray ionization in positive ion mode. On-line desalting and separation from detergents were performed using a Thermo Hypersil-Keystone BetaBasic cyano column (1.0 mm × 10 mm) coupled to the electrospray ionization probe. Aliquots were injected onto the column using at a flow rate of 0.1 mL/min 95% solvent A (0.15% aqueous formic acid) and 5% solvent B (acetonitrile). Gradient elution was performed as follows: 95% A and 5% B from 0 to 1 min, linear gradient to 30% A and 70% B at 6 min, hold at 30% A and 70% B from 6 to 9 min. Electrospray spectra were processed using MassLynx (Waters), and zero-charge state mass spectra were obtained by deconvolution using the MaxEnt1 algorithm.

MALDI mass spectra were generated on a Voyager-DE STR mass spectrometer (Applied Biosystems, Foster City, CA) in positive ion linear mode using sinapinic acid as the matrix. Samples were processed using strong cation exchange ZipTips (ZipTipSCX, Millipore, Billerica, MA) to remove detergent and reversed phase C18 ZipTips for desalting, following the manufacturer's recommended protocols, before spotting the MALDI target.

Enzyme Assays. Xanthine/αKG dioxygenase activity was measured at 25 or 30 °C (as specified in the figure legends) by using the following typical assay conditions (total volume of 1 mL): 1 mM αKG, 40 μM $Fe(NH_4)_2(SO_4)_2$, and 200 μM xanthine in 50 mM MOPS buffer (pH 7.4 or 7.0) (see figure legends). Variations of these conditions included the use of alternate buffers, different pH values, and varied concentrations of substrates. The absorbance at 294 nm was monitored for the assessment of uric acid production ($\epsilon_{294} = 12\,200\ M^{-1}\ cm^{-1}$) with a correction for loss of the xanthine absorbance at this wavelength (measured $\epsilon_{294} = 2000\ M^{-1}\ cm^{-1}$) for an overall change in ϵ_{294} of $10\,200\ M^{-1}\ cm^{-1}$. Units of activity were defined as micromoles of uric acid produced per minute, and the specific activity (units per milligram) was measured as micromoles per minute per milligram of purified XanA.

In addition to the spectroscopic assay described above, xanthine/αKG dioxygenase activity was measured by two alternative methods. Oxygen consumption measurements were carried out in air-saturated MOPS medium (pH 7) at 25 °C by using a Clark-type oxygen electrode. Quantification of αKG consumed during the reaction was assessed by HPLC. Aliquots (300 μL) of the reaction mixtures were quenched by addition of 5 μL of 6 M H_2SO_4; the samples were centrifuged for 5 min at 20000*g*, and the supernatant was chromatographed on an Aminex HPX-87H column (Bio-Rad Laboratories) in 0.013 M H_2SO_4 with detection by using a differential refractometer (Waters, model R401). Succinate was quantified by using a succinate detection kit (Boehringer Mannheim/R-Biopharm) according to the manufacturer's instructions.

Metal Analyses. Particle-induced X-ray emission (PIXE) experiments were carried out in a tandem Pelletron accelerator, using a 3 MeV proton beam with a diameter of 1 mm at the sample surface. The XanA enzyme was dialyzed in 50 mM NH_4HCO_3 and dried on a 3.5 μm Mylar membrane, and the X-ray emission was detected in two solid-state detectors: a Si-pin Amptek (180 eV resolution operated under a helium stream) and for heavier elements a LE Ge detector with a 38 μm Al foil absorber (*20*, *21*). Spectra were collected for 5 min, using at least two sites within each sample. Sulfur was taken as an internal standard, taking into

account that the enzyme subunit contains seven S atoms per polypeptide chain, including two cysteine and five methionine residues. An alternative approach to measuring the iron concentration utilized the $KMnO_4$ oxidation, ascorbate reduction, and ferrozine chelation protocol of Beinert (*22*).

Sources and Synthesis of Chemical Analogues of αKG and Xanthine. αKG, α-ketoadipate, α-ketobutyric acid, pyruvate, phenyl pyruvate, 4-hydroxyphenyl pyruvate, purine, 6-methylpurine, 2-hydroxypurine, 2-hydroxy-6-methylpurine, hypoxanthine, xanthine, 1-methylxanthine, 3-methylxanthine, 7-methylxanthine, 9-methylxanthine, allopurinol, and allantoin were from Sigma-Aldrich. *N*-Oxalylglycine (NOG) was a gift from N. Burzlaff.

8-Hydroxypurine and 6,8-dihydroxypurine (6,8-DHP) were prepared from commercially available (Sigma Aldrich) 4,5-diaminopyrimidine and 4,5-diamino-6-hydroxypyrimidine, respectively, following a modified method described previously (*23*). 2,8-Dihydroxypurine (2,8-DHP) was prepared following a published method (*24*).

[8-^{2}H]Xanthine Preparation. [8-^{2}H]Xanthine was prepared by incubating a 1% (w/v) xanthine solution in ^2H_2O (99.9%, Sigma-Aldrich), with 0.3 M NaO^2H (>99% ^{2}H, Sigma-Aldrich) in a serum vial sealed with a butyl rubber stopper for 20 h in a 100 °C oven. The proton−deuterium exchange was monitored by using NMR spectroscopy to integrate the resonance at 6.9 ppm due to the proton on C-8. The final solution was diluted and neutralized to pH 7.0. The [8-^{2}H]-xanthine precipitated from the solution and was dried under vacuum for at least 3 h. Yields were approximately 90%. The purity of [8-^{2}H]xanthine was monitored by electrospray ionization mass spectrometry, and the level of conversion was shown to be 98.4% as a molar ratio.

^2H_2O Solvent Isotope Effect. In 1 mL of 50 mM MOPS at p^{2}H 8.0 (p^{2}H values were determined by adding 0.4 to the pH 7.6 electrode reading), 0.51 μg of purified XanA was assayed in 40 μM $Fe(NH_4)_2(SO_4)_2$, 1 mM αKG, and 0−200 μM xanthine. All buffers were prepared in ^2H_2O. These data were compared to those from assays carried out under the same conditions at pH 7.6. Of note, the *E. coli*-derived enzyme exhibits optimal activity over a range from pH 7.0 to 8.0.

Fluorescence Spectroscopic Analysis of XanA. Fluorescence measurements were taken on an ISS (Champaign, IL) PC1 spectrofluorimeter. The temperature of the cells was maintained at 30 °C. Fluorescence measurements were carried out at an excitation wavelength of 280 nm (0.5 nm bandwidth) with emission monitored from 300 to 400 nm (2 nm bandwidth).

Structural Modeling. A homology model of XanA was generated on the basis of the structure of the related enzyme TauD (PDB entry 1OTJ, chain A, and PDB entry 1OS7, chain A) (*25*). XanA is 18% identical to TauD over 280 residues and has three significant additional regions of 15, 22, and 18 amino acids. Multiple templates for the XanA structure were obtained with PSI-BLAST (*26*, *27*) starting both from the amino acid sequence of XanA and from that of several closely related proteins for which no structure has yet been reported, and with 3D-Jury (*28*) using the Bioinfo Meta Server (http://bioinfo.pl/Meta). Additional suboptimal alignments for each template were generated using probA (*29*) to produce a large pool of possible models. A structural model was constructed from each alignment, with side chains reconstructed using the MMTSB Tool Set (*30*, *31*), and the best model from the entire set of models was selected according to combined energy scores from DFIRE (*32*), MMGB/SA (*33*), and RAPDF (*34*), using a correlation-based approach (*35*) in combination with clustering. The αKG and iron were placed into the active site according to the TauD structure.

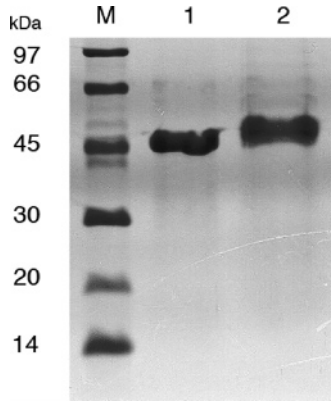

FIGURE 1: SDS−PAGE analysis of the purified XanA from *E. coli* and *A. nidulans*: lane M, markers; lane 1, sample purified from the fungus; lane 2, protein isolated from the bacterium (7 μg each). Stacking and running gels contain 5 and 12% acrylamide.

RESULTS

Purification of XanA from the Bacterial Host. XanA produced in *E. coli* XL1Blue (pxan-His_6) was purified to homogeneity from cell extracts (Figure 1 and Figure S1 of the Supporting Information) by Ni-NTA chromatography. Inclusion of 15% glycerol in the chromatography buffers, which were maintained on ice, helped to minimize protein precipitation during purification. Approximately 5% of the soluble activity was located in the flow-though fractions, perhaps indicating that some XanA interacts tightly with other proteins that fail to bind the resin. As measured by the standard assay protocol, the Ni-NTA column fractions containing purified XanA accounted for 33% of the activity that had been observed in cell extracts. When this pool was treated with 1 mM EDTA at 4 °C for 5 h and then concentrated to 5−12 mg/mL, the activity increased such that 60% of the activity of cell extracts was recovered and yielded a final specific activity for the purified enzyme of 70−80 units/mg of protein at 25 °C which corresponds to a k_{cat} of 49−56 s^{-1} (assuming M_r = 42 000 per subunit). The enzyme recovered from the Ni-NTA column contained 0.26−0.5 mol of Fe/mol of subunit according to the colorimetric assay; that incubated with EDTA lacked detectable Fe, and a sample incubated with exogenous Fe^{II} and then chromatographed on a Sephadex G-25 gel filtration column contained 1.3 mol of Fe/mol of subunit. Concentrated XanA derived from *E. coli* was stable for at least 1 month at 4 °C when stored in 100 mM Tris buffer (pH 8.0) containing 300 mM NaCl, 250 mM imidazole, 1 mM EDTA, and 15% glycerol or at least 2 months if frozen at −80 °C. Additionally, the enzyme was stable for 1 month at 4 °C when stored in 100 mM Tris buffer (pH 7) containing 300 mM NaCl, 250 mM imidazole, 15% glycerol, and 5 μM Fe^{II}.

Purification of XanA from the Fungal Host. In a similar manner, His_6-tagged XanA was purified to homogeneity

(Figure 1) from extracts derived of the *A. nidulans* mycelia by using immobilized metal ion affinity chromatography. To stabilize the enzyme and the activity, 5 μM Fe^{II} was added to the purified enzyme pool. The specific activity of the isolated protein was measured as 22−40 units/mg of protein at 30 °C, equivalent to a k_{cat} of 15.4−30 s^{-1} (again assuming M_r = 42 000 per subunit). Metal analyses by PIXE (Figure S2 of the Supporting Information) indicated 1.13 ± 0.2 mol of Fe/mol of enzyme subunit, with trace levels of Ni and Zn that are likely to derive from the Ni-NTA column and from contamination, respectively. Concentrated XanA derived from *A. nidulans* was stable for at least 5 months at 4 °C when stored in 100 mM Tris buffer (pH 7) containing 300 mM NaCl, 250 mM imidazole, 15% glycerol, and 5 μM Fe^{II}.

Differential Protein Properties of XanA Purified from the Two Host Cells. The SDS−PAGE results described above highlight a key difference between the XanA proteins isolated from the two sources; i.e., the apparent M_r of the *E. coli*-derived protein is larger than that of the protein derived from the fungus (Figure 1). This finding led us to investigate other properties of the two proteins. Efforts to obtain N-terminal sequences were unsuccessful, consistent with the amino termini of both proteins being blocked. Gel filtration chromatography provided an estimated M_r from 39 000 to 42 000 for the native enzyme isolated from the bacterial host (consistent with a monomeric structure); however, similar analysis of the protein from the fungal host showed that it was oligomeric, with an approximate M_r of 500 000 that was consistent with ∼12 subunits per native molecule (Figure S3 of the Supporting Information). The observed differences in the samples hinted at the possibility of unique posttranslational modifications in the proteins produced in the bacterial and eukaryotic hosts.

XanA samples derived from the two sources were each tested for the presence of bound carbohydrate. The protein purified from *A. nidulans*, but not that isolated from *E. coli*, was shown to be glycosylated (Figure 2). It is noteworthy that removal of glycosyl residues from the fungus-derived protein resulted in an apparent molecular mass significantly lower than that of the enzyme isolated from *E. coli*, suggesting a truncation occurs in the fungal host (see below). Specifically, treatment of the native XanA enzyme from *A. nidulans* with the *N*-glycosylase PNGase F led to a shift in the denaturing gel electrophoretic mobility (Figure 2) from a form with an apparent M_r of more than 40 000 to one with an apparent M_r near 33 000, indicating removal of N-glycosylation. The PNGase F-treated protein was still detected by the glycoconjugate immunoassay. These results are consistent with the presence of O-glycosylation in the protein, as well as the N-glycosylation that is removed by PNGase F. As a control, the native and denatured XanA prepared from *E. coli* was subjected to PNGase F treatment, and no shift in mobility was detected in either sample.

In addition, the samples were tested for phosphorylation. Figure S4 (Supporting Information) illustrates the reactions of both proteins with antibodies that recognize specific types of phosphorylated amino acids. The enzyme purified from *E. coli* reacted strongly with both anti-phosphoserine and anti-phosphothreonine antibodies, while the enzyme purified from *A. nidulans* reacted strongly with the anti-phosphothreonine antibodies and only weakly with the antiphosphoserine antibodies. Neither protein sample reacted with anti-phosphotyrosine antibodies.

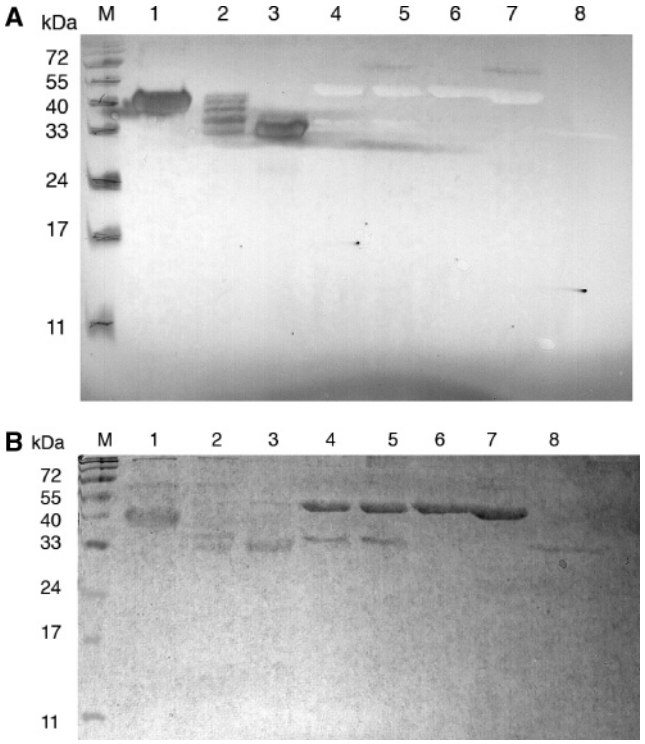

FIGURE 2: Glycosylation analysis of XanA derived from *E. coli* and *A. nidulans*. (A) Protein-linked carbohydrate was detected in XanA samples (5 μg each) by using an immunoassay (DIG glycan detection kit, Roche): lane M, protein size markers (Fermentas); lane 1, XanA purified from *A. nidulans*; lane 2, PNGase F-treated native XanA purified from *A. nidulans*; lane 3, PNGase F-treated XanA from *A. nidulans* after denaturation; lane 4, PNGase F-treated native XanA purified from *E. coli*; lane 5, PNGase F-treated XanA from *E. coli* after denaturation; lanes 6 and 7, XanA from *E. coli*; and lane 8, PNGase F. (B) The same samples were stained for protein with Coomassie blue.

Mass spectrometric methods were used to further characterize the two enzyme forms. Electrospray ionization mass spectrometry of bacterium-derived XanA indicated a single species with a molecular mass of 41 992 Da (data not shown), which matches very well to the theoretical mass (41 996.50 Da; using the ExPASY Compute pI/Mw tool at ca.expasy.org) for the His_6-tagged protein missing its amino-terminal Met residue. This sample provided no evidence of phosphorylation, perhaps arising from subtle differences in bacterial culture conditions in our two different laboratories. In contrast to this single species, the fungus-derived protein sample exhibited a complex electrospray ionization mass spectrum centered near 36 000 Da (Figure 3), in agreement with the results from matrix-assisted laser desorption ionization mass spectrometry (data not shown). The spectrum of Figure 3 includes features separated by 162 mass units, consistent with glycosylation involving hexose sugars, as well as features separated by 80 mass units, indicating phosphorylation. The smallest component of the spectrum exhibits a mass of 35 171 Da, indicating that the nonglycosylated and nonphosphorylated fungal protein is severely truncated compared to the theoretical mass of the full-length protein (42 127.69 Da). This truncation, consisting of approximately 60 residues, must occur at the N-terminus, since the C-terminal His_6 tag was used for enzyme purification.

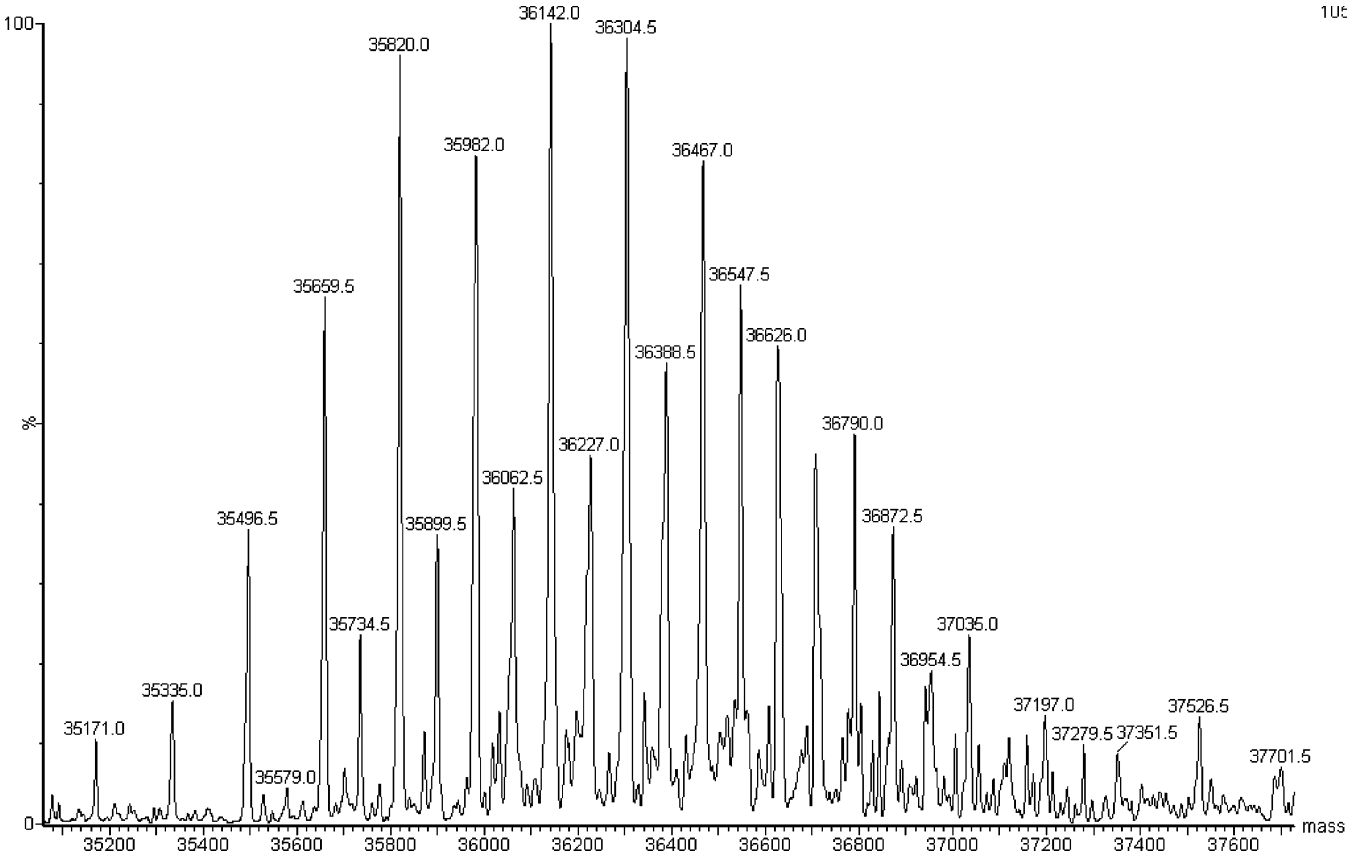

FIGURE 3: Mass spectrometric analysis of fungus-derived XanA. The XanA protein isolated from *A. nidulans* was analyzed by electrospray ionization mass spectrometry. The figure depicts a series of peaks separated by 162 and 80 mass units, consistent with glycosylation and phosphorylation, respectively.

Effects of pH on the Stability and Activity of Xanthine/αKG Dioxygenase. The effect of pH on the stability of XanA was examined for the enzyme isolated from each source. After the XanA samples were incubated in various pH buffers at 4 °C for 3 h, the activity remaining was examined by using the standard assay procedure. The results (data not shown) indicate that each purified enzyme is stable over a wide pH range (7.0−11.0).

Two methods were used to examine the effects of pH on the activity of the two enzyme forms. XanA isolated from *E. coli* was assayed by using a series of different buffers and shown to exhibit a narrow pH optimum of 7.0−8.0 with pH 7.4 yielding optimal activity for Tris, MOPS, MES, imidazole, and HEPES buffers (Figure S5, top panel, Supporting Information). For the XanA isolated from *A. nidulans*, a constant ionic strength, three-buffer system containing 0.1 M MOPS, 0.52 M Tris, and 0.052 M ethanolamine (*36*) provided a sharp maximal activity at pH 7.0 (Figure S5, bottom panel).

Kinetic Analyses and Stoichiometry of XanA. The kinetic parameters were very similar for XanA isolated from the two sources. For the *E. coli*-derived enzyme, the results of studies using varied αKG concentrations provided a K_m of 31.1 ± 1.6 μM and a k_{cat} of 66.5 s^{-1} at 25 °C (Figure 4A), while those for varied xanthine concentrations provided a K_m of 45.2 ± 3.6 μM and a k_{cat} of 71.4 s^{-1} (Figure 4B). Similarly, when the protein isolated from the *A. nidulans* enzyme was assayed at 30 °C with varied αKG or xanthine concentrations, the measured K_m values were 50 ± 6 and 46 ± 4 μM, respectively, but with a smaller k_{cat} that ranged from 15 to 30 s^{-1} depending on the preparation.

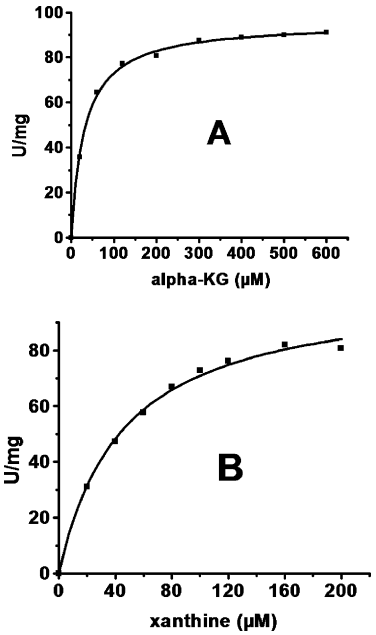

FIGURE 4: Substrate and cosubstrate concentration dependencies of XanA. The effects of varying the concentrations of (A) αKG and (B) xanthine on xanthine/αKG dioxygenase activity were examined for the *E. coli*-derived protein at 25 °C. Except for the compound being varied, the assay solutions contained 40 μM Fe^{II}, 1 mM αKG, and 200 μM xanthine in 50 mM MOPS buffer (pH 7.4). The data were fit to the Michaelis−Menten equation.

The stoichiometry of the enzymatic reaction was examined for XanA from each source. Using the fungus-derived protein, the degradation of 120 μM xanthine was ac-

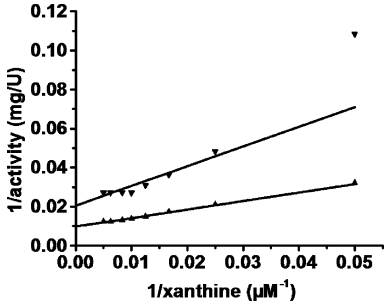

FIGURE 5: Solvent deuterium isotope effect on XanA activity. The effects of varying the concentration of xanthine on xanthine/αKG dioxygenase activity were examined at 25 °C in 50 mM MOPS buffer at p^{2}H 8.0 (▼) (p^{2}H values were determined by adding 0.4 to the pH electrode reading) or pH 7.6 (▲) containing 40 μM Fe^{II}, 1 mM αKG, and 0−200 μM xanthine.

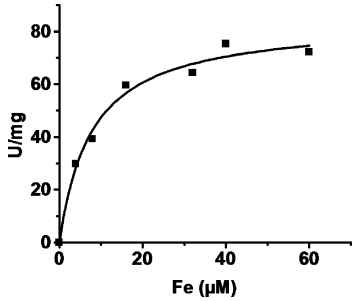

FIGURE 6: Fe^{II} concentration dependence of XanA. The effects of varying the concentration of Fe^{II} on xanthine/αKG dioxygenase activity were examined by using the *E. coli*-derived protein at 25 °C in solutions containing 1 mM αKG and 200 μM xanthine in 50 mM MOPS buffer (pH 7.4).

companied by the production of 110 μM uric acid, and this coincided with the consumption of 130 μM oxygen and the production of 185 μM succinate. The larger changes in the amount of oxygen and succinate compared to those of xanthine and uric acid are consistent with a well-known phenomenon reported for this class of enzymes in which substrate hydroxylation can be partially uncoupled from oxidative decarboxylation (*37*−*40*). An analogous near coincidence between xanthine consumption, uric acid production, and oxygen consumption was observed for the bacterium-derived sample (results not shown).

Isotope Effects. To test for substrate or solvent isotope effects on the overall reaction rate, activity assays were carried out by using [8-^{2}H]xanthine or in ^2H_2O and compared to control studies with unlabeled xanthine in H_2O. No significant isotope effect was observed when the reaction was carried out with [8-^{2}H]xanthine (98.4% enriched with ^{2}H) and compared to nonlabeled substrate (data not shown). In contrast, a significant solvent deuterium isotope effect was observed (Figure 5), with the V_{max} reduced by 50% (72.1 units/mg dropping to 34.0 units/mg) and the K_m nearly unaffected (45.2 and 48.9 mM, respectively).

Metal Ion Dependence of XanA. The metal dependence of the reaction was examined with enzyme samples derived from the two sources. Fe^{II} is required for xanthine/αKG dioxygenase activity, with half-maximal activity at ∼7 μM when the apoprotein isolated from the bacterium is used (Figure 6). Depending on the experimental conditions, Fe^{II} concentrations of >25 μM can lead to enzyme inhibition of XanA isolated from *E. coli*, whereas the enzyme from *A. nidulans* was not inhibited at Fe^{II} concentrations up to 80 μM.

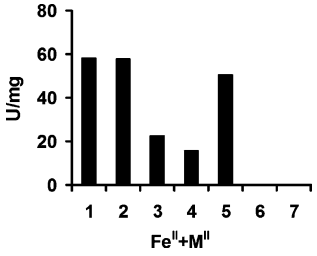

FIGURE 7: Divalent cation inhibition of XanA. The effects of several divalent cations (M^{II}, at 40 μM) on xanthine/αKG dioxygenase activity were examined by using the *E. coli*-derived protein at 25 °C in solutions containing 40 μM Fe^{II}, 1 mM αKG, and 200 μM xanthine in 50 mM MOPS buffer (pH 7.4): (1) Fe^{II} only and Fe^{II} with (2) Mg^{II}, (3) Mn^{II}, (4) Co^{II}, (5) Ni^{II}, (6) Zn^{II}, or (7) Cu^{II}.

Metal ions other than Fe^{II} were tested and found to be unable to stimulate activity when added to the apoprotein (data not shown). When various metal ions were added to the assay buffer in concentrations equivalent to that of Fe^{II}, both Cu^{II} and Zn^{II} completely inhibited the xanthine/αKG dioxygenase activity, with partial inhibition observed with Co^{II}, Mn^{II}, and (much less pronounced) Ni^{II} (Figure 7). The inactive metal ions are presumed to compete for the Fe^{II}-binding site.

Effect of Salt on XanA Activity. The activity of XanA isolated from the bacterial source was shown to decrease in buffers containing NaCl (Figure S6 of the Supporting Information). Kinetic analyses revealed that 0.5 M NaCl increased the K_m of αKG to 0.74 ± 0.08 mM, increased the K_m of xanthine to 105 ± 5.8 μM, and decreased the k_{cat} to 35.4 and 43.2 s^{-1}, respectively, in the two studies. These findings indicate that the K_m of αKG is significantly affected by ionic strength, while the K_m of xanthine and k_{cat} are less affected, and demonstrate that the salt content of fractions recovered during protein isolation must be considered when the enzyme is assayed.

αKG Analogues. In addition to αKG, α-ketoadipic acid is a cosubstrate of XanA and results in an activity of 9.2 units/mg of protein or $\sim^1/_{10}$ of that observed with αKG, when examined using the *E. coli*-derived protein. Kinetic analyses revealed a k_{cat} of 7.6 s^{-1} and a K_m of 0.16 mM for this alternative cosubstrate compared to a k_{cat} of 61 s^{-1} and a K_m of 31 μM for αKG. In contrast, pyruvate, α-ketobutyric acid, phenyl pyruvate, and 4-hydroxyphenyl pyruvate were not used as cosubstrates. NOG, a known inhibitor of several Fe^{II}/αKG-dependent dioxygenase family members (*41*−*45*), was shown to compete with αKG and provided a K_i of 0.12 μM for inhibition when tested with the bacterium-derived enzyme (Figure 8).

Xanthine Analogues. XanA was shown to be highly specific for xanthine. On the basis of the spectroscopic assay using standard conditions with 12 nM enzyme, no activity was detected when the enzyme was assayed with 80, 100, or 200 μM hypoxanthine, 1-methylxanthine, 3-methylxanthine, 7-methylxanthine, 9-methylxanthine, purine, 6-methylpurine, 2-hydroxypurine, 8-hydroxypurine, 2,8-dihydroxypurine, 2-hydroxy-6-methylpurine, allopurinol, allantoin, or adenosine diphosphate. Similarly, significant inhibitory effects were not observed with any of these compounds at 100 or 200 μM (although very modest inhibition was noted with

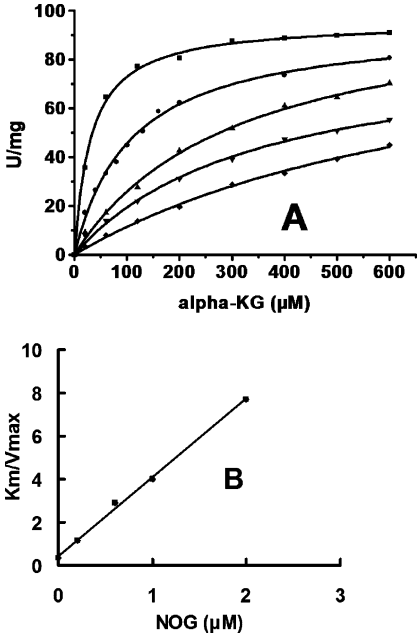

FIGURE 8: NOG inhibition of XanA. (A) The effects of varying concentrations of NOG (0, 0.2, 0.6, 1.2, and 2 μM) on xanthine/αKG dioxygenase activity were examined by using the *E. coli*-derived protein at 25 °C in solutions containing 40 μM Fe^{II}, 1 mM αKG, and 200 μM xanthine in 50 mM MOPS buffer (pH 7.4). Each set of initial rate data was fit to the Michaelis−Menten equation. (B) Replot of the values of the apparent K_m divided by the apparent V_{max} as a function of inhibitor concentration.

2,8-DHP). The one xanthine-like compound that does significantly inhibit the enzyme but does not serve as a substrate is 6,8-DHP. When bacterium-derived XanA was assayed by using standard conditions supplemented with 80 μM 6,8-DHP, the activity decreased by 24% when the reaction was initiated by enzyme addition or by 60% if the reaction was initiated by adding xanthine. Fungus-derived XanA appeared to be even more sensitive to the presence of this inhibitor (data not shown). Although the kinetic mechanism of inhibition by this compound currently is unclear, the affinity of the enzyme samples for this compound was further examined by fluorescence measurements.

Fluorescence Spectroscopic Analysis of XanA. The binding of αKG, xanthine, and 6,8-DHP to both the bacterium- and fungus-derived proteins was examined by monitoring changes in the endogenous fluorescence of the proteins (Figure S7 of the Supporting Information). Fitting of the plots of the change in fluorescence intensity versus ligand concentration revealed that the two proteins exhibited very similar K_d values for xanthine (110 ± 19 and 220 ± 19 μM for the bacterium- and fungus-derived samples, respectively), αKG (29 ± 4 and 17 ± 4 μM, respectively), and 6,8-DHP (60.5 ± 9 and 156 ± 16 μM, respectively). Interestingly, the αKG K_d happens to be very similar to the K_m of this compound measured during catalysis. The measured K_d of 6,8-DHP confirms that this compound binds to the protein even in the absence of Fe^{II} and αKG.

Homology Model of XanA. XanA was aligned with TauD, and the structure of that protein (*25*, *46*) was used as the template to create a homology model. The overall level of sequence identity is 18%; however, the level of sequence identity of the most relevant structural regions near the active site is 33%. Moreover, given recent advances in structure

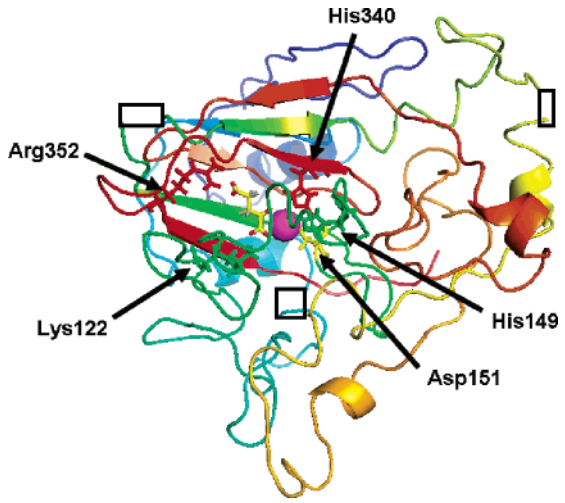

FIGURE 9: Homology model of XanA. Ribbon diagram depicting the XanA homology model predicted by using TauD (PDB entry 1OS7, A chain) as a template. The polypeptide chain is colored from blue to red (N-terminus to C-terminus) with gaps indicated by boxes for the nonmodeled loops involving residues 72−88, 173−190, and 219−231. The postulated metal ligands (His149, Asp151, and His340) are colored green, yellow, and red, respectively, to the right of the magenta Fe^{II} sphere. Bound αKG (yellow) chelates the metals and is suggested to be stabilized by a salt bridge to the C-5 carboxylate involving Arg352 (red) and a hydrogen bond to the C-1 carboxylate via Lys122 (green).

prediction, levels of sequence identity as low as 18% are commonly sufficient to support comparative modeling with a good match of predicted secondary structure elements (*47*, *48*) as in the case of XanA. Consequently, it is reasonable to assume that our model of the XanA structure captures the overall features correctly, while structural details near the active site are likely represented more accurately. Nevertheless, we acknowledge that any predicted model without further experimental validation remains speculative and is subject to some level of uncertainty.

As illustrated in Figure 9, the XanA protein is predicted to contain the double-stranded β-helix fold comprised of eight β-strands with connecting loops, which is typical for this enzyme family (*6*, *49*). Three loops in the sequence, comprising residues 72−88, 173−190, and 219−231, had no counterparts in TauD and were not modeled (indicated by boxes at the appropriate positions in the figure), but these are all distant from the putative active site region. The homology model contains the Fe^{II}-binding site (His149, Asp151, and His340) expected from prior sequence alignments (*2*). The cosubstrate (colored yellow) was positioned into the model to chelate Fe^{II} in a similar fashion as αKG occurs in TauD. The αKG C-5 carboxylate is predicted to form a salt bridge with Arg352 (colored red), while Lys122 (colored green) is well positioned to stabilize the C-1 carboxylate of the cosubstrate.

DISCUSSION

In this study, we describe the isolation and general characterization of xanthine/αKG dioxygenase, a novel enzyme found exclusively in the fungal kingdom (*2*). Immobilized metal ion chromatography proved to be very effective for purifying recombinant XanA from either the bacterial or fungal host cells. As described below, the two forms of the protein differed markedly in their properties but were very similar in their enzymatic properties.

Posttranslational Modifications. Our comparison of recombinant XanA purified from *E. coli* and *A. nidulans* reveals very different quaternary structures and posttranslational modifications. Whereas the protein derived from the bacterial source is a monomer, that isolated from the fungus is much larger, with an apparent M_r of 500 kDa. Both protein samples are at least partially phosphorylated, but the sample from the fungus is also glycosylated. Treatment of the latter protein with PNGase F results in a dramatic shift in electrophoretic mobility, but not all glycosylation is removed by this process, indicating the presence of both N- and O-glycoconjugates. The smaller electrophoretic species is consistent with the size of the protein determined by mass spectrometric methods. These results suggest an extensive truncation takes place at the N-terminus of the fungus-derived enzyme. Analogous biochemical comparisons between the enzyme form isolated from its native eukaryotic host and the form isolated from a heterologous host, such as the *E. coli* used here, have not been reported for other Fe^{II}/αKG dioxygenase family members.

An extant question is the role of the extensive N-terminal processing of enzyme isolated from its natural fungal host. We speculate that this feature may relate to cellular targeting of the XanA enzyme. It is not unreasonable to propose that an oxidoreductase such as XanA could be peroxisomal. In fact, the immediate downstream enzyme, urate oxidase, has been shown to be peroxisomal in every organism where its localization has been investigated, including amoebas, mammals, and plants (*50*−*53*). A urate oxidase−green fluorescent protein fusion shows a particulate intracellular distribution in *A. nidulans*, fully consistent with a peroxisomal localization (G. Langousis and G. Diallinas, unpublished data). XanA does not possess a C-terminal peroxisomal targeting signal (variations of an SKL tripeptide, denoted PTS1); however, it contains a RSALYTHL sequence (residues 40−47) that resembles the PTS2 N-terminal import sequence (variations of RLX_5HL) found in a minority of peroxisomal proteins throughout the eukaryotes (*54*−*56*). In some instances, including mammalian (*57*), yeast (*58*), and plant (*59*) peroxisomal proteins, it has been shown that PST2 is contained in a pre-sequence that is cleaved upon peroxisomal entry. The function of XanA glycosylation could be understood in this context as a mechanism for protecting the protein from further proteolysis.

Insights into the Posttranslational Modifications from the XanA Homology Model. The XanA homology model (Figure 9) provides useful insights into the likely sites of posttranslational modification (Figure S8 of the Supporting Information). The model is based on the full-length sequence, but we assume the overall fold is maintained even in the truncated version derived from the fungal host because this extension is external to the double-stranded β-helix core. Consistent with our PNGase F results that demonstrate the presence of N-glycosylation sites in the fungus-derived protein, the NetNGlyc 1.0 server (R. Gupta, E. Jung, and S. Brunak, unpublished) predicts glycosylation of Asn118, and the model places this residue on the protein surface. The PNGase F-treated fungal-derived protein still stains as a glycoprotein, consistent with O-linked glycoconjugates in the protein. Thr5 and Thr10 are predicted to be glycosylated by the NetOGlyc 3.1 server (*60*), while the YingOYang 1.2 server (R. Gupta, J. Hansen, and S. Brunak, unpublished) predicts Thr5, Ser37, Thr195, Ser231, and Ser316 as possible sites of glycosylation. The XanA homology model has these positions surface exposed except for Thr195. On the basis of our mass spectrometry results showing truncation of approximately 60 residues from the N-terminus, we suggest Ser231 or Ser316 as the most likely site of O-glycosylation.

A wide range of potential Ser, Thr, or Tyr phosphorylation sites are identified in XanA by the NetPhos 2.0 server (*61*) and by Prosite (www.expasy.org). Phosphoproteins are common in eukaryotes and are well-known in *E. coli* (*62*). Thr phosphorylation sites are predicted by at least one program to include Thr5, Thr38, Thr58, Thr66, Thr120, Thr177, and Thr274. The first three residues are missing in the fungus-derived protein on the basis of the mass spectrometry results. The homology model predicts that Thr66 and Thr120 are buried, whereas the other residues are exposed to the surface. The bacterium-derived protein also reacts with antibodies directed against phosphoserine, whereas XanA derived from the fungus reacted only weakly with these antibodies. We attribute this difference in reactivity between the two proteins to the phosphorylation site being inaccessible in the fungus-derived sample, due to nearby glycosylation or the fact that the site is located at a subunit interface in the multimeric protein. Predicted sites of Ser phosphorylation include Ser15, Ser37, Ser142, Ser184, Ser199, Ser208, Ser217, Ser218, and Ser341. The first two residues are absent in the fungus-derived protein. Residues Ser199 and Ser341 are predicted to be somewhat buried in the model; Ser184 occurs on a loop that could not be modeled, and the other residues are predicted to be surface-exposed. Of note, Ser341 would be made more inaccessible by glycosylation of Thr195, thus potentially explaining the source specificity behavior for Ser phosphorylation.

General Aspects of XanA Activity. Purified XanA is unstable at room temperature (denaturing within 1 h even in buffers containing 15% glycerol), when agitated (e.g., during stirring in an Amicon concentrator), or when incubated at pH <6.5 (the pI estimated for XanA is 5.82 according to the ExPASy ProtParam tool at ca.expasy.org). EDTA treatment enhances the activity of the highly concentrated bacterium-derived enzyme, and this compound is maintained in the storage buffer to ensure the maximal lifetime of the activity. We attribute the enhancement effect of EDTA to its ability to remove inhibitory Ni^{II} (coeluted with the enzyme from the NTA resin) and Fe^{III} (the oxidized, inactive state of the metal) from the enzyme so that the apoprotein can bind Fe^{II} in the assay buffer. Several other Fe^{II}/αKG dioxygenases are purified as their apoprotein forms by inclusion of chelators (*63*, *64*). In contrast, some representatives of these enzymes have been purified anaerobically to ensure that the metal remains in its reduced form (*65*, *66*).

The kinetic properties of XanA as purified from *E. coli* (∼70 units/mg, K_m of 31 μM for αKG, and K_m of 45 μM for xanthine at pH 7.4) compare well with those of XanA isolated from *A. nidulans* (30 units/mg, and K_m values of 50 and 46 μM, respectively, at pH 7.0), and these results are compatible with those reported earlier for the enriched sample from the fungus (40 units/mg, 50 μM, and 23 μM, respectively) (*2*). Although the xanthine C−H bond is broken at C-8 during turnover, substitution of the proton at this position with ^2H did not lead to a substrate isotope effect. This result

demonstrates that C−H cleavage is not the rate-determining step in the reaction. The deuterated substrate might be useful in future experiments in examining individual steps in the reaction by using transient kinetic approaches, as elegantly demonstrated with deuterated substrate and stopped-flow techniques for TauD (*67*) and, more recently, prolyl 4-hydroxylase (*68*). In contrast to the situation with labeled xanthine, a solvent isotope effect was observed upon substitution of H_2O with D_2O (Figure 5). This substitution had little effect on the K_m of xanthine while decreasing V_{max} by 40% compared to the assay in H_2O. This result suggests that a chemical group possessing an exchangeable proton is important in the rate-determining step of the overall reaction. Options for the protonatable group include a general base or general acid protein side chain or a metallocenter species such as Fe^{III}-OOH or Fe^{III}-OH. The finding of a solvent deuterium isotope effect contrasts with the case of TauD, where product release is the slow step in catalysis and no solvent isotope effect is observed (*12*, *63*).

The reaction requires Fe^{II} (half-maximal activity at 7 μM for standard conditions), consistent with the results of related family members. Zn^{II} and Cu^{II} are potent inhibitors of XanA, and several other metals also inhibit the enzyme (Figure 7). This situation resembles that known for related enzymes such as TauD where Co^{II} and Ni^{II} inhibition has been studied (*41*), clavaminate synthase where Co^{II} inhibition was characterized (*69*), or TfdA where the Cu^{II}-inhibited enzyme was analyzed (*70*). The inhibitory metal ions are likely to substitute for Fe^{II} and presumably utilize the same set of amino acid side chain ligands.

The inhibitory effects of NaCl on XanA observed here represent, to the best of our knowledge, the only systematic characterization of any salt effect on an Fe^{II}/αKG dioxygenase. The presence of salt leads to a large increase in the K_m of αKG, a small increase in the K_m of xanthine, and a reduction in k_{cat}. We attribute the K_m effect to the ability of salt to interfere with salt bridge formation and other stabilizing interactions between αKG or xanthine and the protein. Similar salt effects are likely to apply to a wide range of other family members; thus, one must exercise caution in the choice of ionic strength when conducting enzyme assays.

Cosubstrate and Substrate Specificity. The cosubstrate specificity of XanA is somewhat more relaxed than that for the primary substrate, with α-ketoadipic acid (with one extra carbon compared to αKG) also yielding activity. The increase in K_m and the decrease in k_{cat} for the incorrectly sized analogue are easily rationalized in terms of the XanA homology model, where both the C-1 and C-5 carboxylates of αKG are predicted to interact with the protein (with Lys122 and Arg352, respectively) while also chelating the active site metal ion. Alternative α-keto acids are known to support αKG-dependent activities of several other enzyme family members, including TauD, TfdA, RdpA, SdpA, and an alkyl sulfatase (*11*, *64*, *71*, *72*). The αKG homologue NOG is a competitive inhibitor of XanA (Figure 8), consistent with its known inhibition of several other representatives of the Fe^{II}/αKG-dependent hydroxylases. Of interest, the measured K_i of NOG for XanA (0.12 μM) is well below the K_m of αKG in this enzyme and much below the reported K_i of 290 μM for inhibition of TauD (*41*). More generally, the K_i of NOG can vary widely among family members [e.g., it is reported to be 1.9−7.0 μM for collagen prolyl 4-hydroxylase (*42*) and 1.2 mM for an oxygen-sensing asparaginyl hydroxylase (*45*)], presumably due to distinct interactions with the active site protein side chains in the target enzymes.

XanA proved to be exquisitely specific to its primary substrate. For example, allopurinol [a known substrate and inhibitor of xanthine oxidase (*73*)], 1-methylxanthine and 2-hydroxy-6-methylpurine [alternative substrates of the Moco-containing enzyme (*74*, *75*)], and several other purine-type compounds were neither substrates nor inhibitors of XanA. Of the compounds that were tested, only 6,8-DHP bound tightly to the enzyme. For comparison, other members of the Fe^{II}/αKG-dependent dioxygenase family range widely in their substrate specificities. The prolyl hydroxylases involved in the hypoxic response appear to be highly specific in recognizing a single prolyl residue in the HIF1α protein (*76*, *77*). By contrast, TfdA utilizes a wide range of phenoxyacetic acids (*64*) and a yeast αKG/sulfonate dioxygenase metabolizes a diverse array of sulfonates (*78*).

Insights into Substrate Binding from the XanA Homology Model. Additional structural or mutagenesis studies are required to characterize the mode of substrate binding to XanA; however, our homology model (Figure 9) allows us to identify potential key active site residues (Figure S9 of the Supporting Information). The model depicts a pocket adjacent to the metallocenter and lined by a series of putative active site residues (Gln99, Pro100, Gln101, Ile110, Thr120, Lys122, Glu137, Ala152, Leu154, Gln356, and Asn358) that are generally well conserved in sequences of XanA orthologues (Figure S10 of the Supporting Information). Pro100, Gln101, Gln356, and Asn358 are universally conserved in XanA sequences. Gln99 counterparts are often present, but Val occupies this position in some representatives. Lys122, which could stabilize the αKG C-1 carboxylate as well as bind substrate, is either retained or conservatively replaced with Arg or Thr. In some fungi, various residues (Lys, Gln, Arg, Asn, and Glu) replace Thr120, but all of these are able to function in hydrogen bonding. Similarly, Asp, Gln, or Ser, each capable of similar hydrogen bond interactions, replaces Glu137 in other XanA homologues. Among the hydrophobic residues predicted to surround the active site, Ile110 is replaced with Val or Phe, Ala152 is replaced with Ser in one case, Leu154 is strictly conserved, and Leu251 (for clarity, this is not shown in Figure S9 because it lies on top of Pro100) is retained or replaced by other large side chains in other orthologues. Aromatic groups, often involved in $\pi-\pi$ stacking interactions with nucleic acids and known to occur in xanthine hydroxylase (*8*, *79*) and uric acid oxidase (*80*), do not appear to be important for binding xanthine in xanthine/αKG dioxygenase on the basis of this model. These predictions set the stage for future chemical modification, mutagenesis, and structural efforts aimed at examining the substrate binding interactions.

ACKNOWLEDGMENT

We thank Mario Calcagno for providing laboratory facilities to G.M.M.-M., Antonietta Cultrone for generous help at the outset of this work, Christine Drevet for the alignment of XanA with putative orthologous sequences from several fungi, and Nicolai Burzlaff for providing NOG. We also give thanks for the generous help of José L. Ruvalcaba-Sil for

the PIXE analyses, Laura Palomares for the glycosylation analyses, Guillermo Mendoza-Hernandez for the N-terminal Edman degradation analyses, Dan Jones for mass spectrometry assistance, and George Diallinas for allowing us to quote unpublished data from his laboratory.

SUPPORTING INFORMATION AVAILABLE

Methods related to cloning for overproduction of XanA as a His-tagged protein in *A. nidulans* and *E. coli* and for purification of protein from each source, 10 figures and their accompanying legends, and coordinate file in PDB format for the XanA homology model. This material is available free of charge via the Internet at http://pubs.acs.org.

REFERENCES

1. Hille, R. (2005) Molybdenum-containing hydroxylases, *Arch. Biochem. Biophys. 433*, 107−116.
2. Cultrone, A., Scazzocchio, C., Rochet, M., Montero-Moràn, G., Drevet, C., and Fernàndez-Martìn, R. (2005) Convergent evolution of hydroxylation mechanisms in the fungal kingdoms: Molybdenum cofactor-independent hydroxylation of xanthine via α-ketoglutarate dependent dioxygenase, *Mol. Microbiol. 57*, 276−290.
3. Darlington, A. J., and Scazzocchio, C. (1968) Evidence for an alternative pathway of xanthine oxidation in *Aspergillus nidulans*, *Biochim. Biophys. Acta 166*, 557−568.
4. Sealy-Lewis, H. M., Scazzocchio, C., and Lee, S. (1978) A mutation defective in xanthine alternative pathway of *Aspergillus nidulans*: Its use to investigate the specificity of *uaY* mediated induction, *Mol. Gen. Genet. 164*, 303−308.
5. Cultrone, A., Reyes-Dominguez, Y., Drevet, C., Scazzocchio, C., and Fernàndez-Martìn, R. (2007) The tightly regulated promoter of the *xanA* gene of *Aspergillus nidulans* is included in a helitron, *Mol. Microbiol. 63*, 1577−1587.
6. Hausinger, R. P. (2004) Fe(II)/α-ketoglutarate-dependent hydroxylases and related enzymes, *Crit. Rev. Biochem. Mol. Biol. 39*, 21−68.
7. Glatigny, A., Hof, P., Romao, M. J., Huber, R., and Scazzocchio, C. (1998) Altered specificity mutations define residues essential for substrate positioning in xanthine dehydrogenase, *J. Mol. Biol. 278*, 431−438.
8. Truglio, J. J., Theis, K., Leimkühler, S., Rappa, R., Rajagopalan, K. V., and Kisker, C. (2002) Crystal structure of the active and alloxanthine-inhibited forms of xanthine dehydrogenase from *Rhodobacter capsulatus*, *Structure 10*, 115−125.
9. Goudela, S., Karatza, P., Koukaki, M., Frilingos, S., and Diallinas, G. (2005) Comparative substrate recognition by bacterial and fungal purine transporters of the NAT/NCS2 family, *Mol. Membr. Biol. 22*, 263−275.
10. Koukaki, M., Vlanti, A., Goudela, S., Pantazopoulou, A., Gioule, H., Tournaviti, S., and Diallinas, G. (2005) The nucleobase-ascorbate transporter (NAT) signature motif in UapA defines the function of the purine translocation pathway, *J. Mol. Biol. 350*, 499−513.
11. Eichhorn, E., van der Ploeg, J. R., Kertesz, M. A., and Leisinger, T. (1997) Characterization of α-ketoglutarate-dependent taurine dioxygenase from *Escherichia coli*, *J. Biol. Chem. 272*, 23031−23036.
12. Grzyska, P. K., Ryle, M. J., Monterosso, G. R., Liu, J., Ballou, D. P., and Hausinger, R. P. (2005) Steady-state and transient kinetic analyses of taurine/α-ketoglutarate dioxygenase: Effects of oxygen concentration, alternative sulfonates, and active site variants on the Fe(IV) intermediate, *Biochemistry 44*, 3845−3855.
13. Saari, R. E., and Hausinger, R. P. (1998) Ascorbic acid-dependent turnover and reactivation of 2,4-dichlorophenoxyacetic acid/α-ketoglutarate dioxygenase using thiophenoxyacetic acid, *Biochemistry 37*, 3035−3042.
14. Liu, A., Ho, R. Y. N., Que, L., Jr., Ryle, M. J., Phinney, B. S., and Hausinger, R. P. (2001) Alternative reactivity of an α-ketoglutarate-dependent iron(II) oxygenase: Enzyme self-hydroxylation, *J. Am. Chem. Soc. 123*, 5126−5127.
15. Ryle, M. J., Liu, A., Muthukumaran, R. B., Ho, R. Y. N., Koehntop, K. D., McCracken, J., Que, L., Jr., and Hausinger, R. P. (2003) O_2- and α-ketoglutarate-dependent tyrosyl radical formation in TauD, an α-keto acid-dependent non-heme iron dioxygenase, *Biochemistry 42*, 1854−1862.
16. Henshaw, T. F., Feig, M., and Hausinger, R. P. (2004) Aberrant activity of the DNA repair enzyme AlkB, *J. Inorg. Biochem. 98*, 856−861.
17. Bradford, M. M. (1976) A rapid and sensitive method for the quantitation of microgram quantities of protein utilizing the principle of protein-dye binding, *Anal. Biochem. 72*, 248−254.
18. Laemmli, U. K. (1970) Cleavage of structural proteins during the assembly of the head of bacteriophage T4, *Nature 227*, 680−685.
19. Maley, F., Trimble, R. B., Tarentino, A. L., and Plummer, T. H., Jr. (1989) Characterization of glycoproteins and their associated oligosaccharides through the use of endoglycosidases, *Anal. Biochem. 180*, 195−204.
20. Garman, E. (1999) Leaving no element of doubt: Analysis of proteins using microPIXE, *Structure 7*, R291−R299.
21. Garman, E. F., and Grime, G. W. (2005) Elemental analysis of proteins by microPIXE, *Prog. Biophys. Mol. Biol. 89*, 173−205.
22. Beinert, H. (1978) Micro methods for the quantitative determination of iron and copper in biological material, *Methods Enzymol. 54*, 435−445.
23. Albert, A., and Brown, D. J. (1954) Purine studies. Part I. Stability to acid and alkali. Solubility. Ionization. Comparison with pteridines, *J. Chem. Soc.*, 2060−2071.
24. Dornow, A., and Hinz, E. (1958) Syntheses of nitrogen-containing heterocycles. XVIII. Ortho-condensations of heterocyclic *o*-aminocarboxylic acid derivatives, *Chem. Ber. 91*, 1834−1840.
25. O'Brien, J. R., Schuller, D. J., Yang, V. S., Dillard, B. D., and Lanzilotta, W. N. (2003) Substrate-induced conformational changes in *Escherichia coli* taurine/α-ketoglutarate dioxygenase and insight into the oligomeric structure, *Biochemistry 42*, 5547−5554.
26. Altschul, S. F., Madden, T. L., Schaffer, A. A., Zhang, J. H., Zhang, Z., Miller, W., and Lipman, D. J. (1997) Gapped BLAST and PSI-BLAST: A new generation of protein database search programs, *Nucleic Acids Res. 25*, 3389−3402.
27. Schäffer, A. A., Aravind, L., Madden, T. L., Shavirin, S., Spouge, J. L., Wolf, Y. I., Koonin, E. V., and Altschul, S. F. (2001) Improving the accuracy of PSI-BLAST protein database searches with composition-based statistics and other refinements, *Nucleic Acids Res. 29*, 2994−3005.
28. Ginalski, K., Elofsson, A., Fisher, D., and Rychlewski, L. (2003) 3D-Jury: A simple approach to improve protein structure predictions, *Bioinformatics 19*, 1015−1018.
29. Muckstein, U., Holfacker, I. L., and Stadler, P. F. (2002) Stochastic pairwise alignments, *Bioinformatics 18* (Suppl. 2), S153−S160.
30. Feig, M., Rotkiewicz, P., Kolinski, A., Skolnick, J., and Brooks, C. L., III (2000) Accurate reconstruction of all-atom protein representations from side-chain-based low-resolution models, *Proteins 41*, 86−97.
31. Feig, M., Karanicolas, J., and Brooks, C. L., III (2004) MMTSB tool set: Enhanced sampling and multiscale modeling methods for applications in structural biology, *J. Mol. Graphics Modell. 22*, 377−395.
32. Zhang, C., Liu, S., Zhu, Q. Q., and Zhou, Y. Q. (2005) A knowledge-based energy function for protein-ligand, protein-protein, and protein-DNA complexes, *J. Med. Chem. 48*, 2325−2335.
33. Feig, M., and Brooks, C. L., III (2002) Evaluating CASP4 predictions with physical energy functions, *Proteins: Struct., Funct., Genet. 49*, 232−245.
34. Samudrala, R., and Moult, J. (1998) An all-atom distance-dependent conditional probability discriminatory function for protein structure prediction, *J. Mol. Biol. 275*, 895−916.
35. Stumpff-Kane, A. W., and Feig, M. (2006) A correlation-based method for the enhancement of scoring functions on funnel-shaped energy landscapes, *Proteins: Struct., Funct., Bioinf. 63*, 155−164.
36. Ellis, K. J., and Morrison, J. F. (1982) Buffers of constant ionic strength for studying pH-dependent processes, *Methods Enzymol. 87*, 405−426.
37. Counts, D. F., Cardinale, G. J., and Udenfriend, S. (1978) Prolyl hydroxylase half reaction: Peptidyl prolyl-independent decarboxylation of α-ketoglutarate, *Proc. Natl. Acad. Sci. U.S.A. 75*, 2145−2149.
38. Rao, N. V., and Adams, E. (1978) Partial reaction of prolyl hydroxylase. $(Gly\text{-}Gly\text{-}Pro)_n$ stimulates α-ketoglutarate decarboxylation without prolyl hydroxylase, *J. Biol. Chem. 253*, 6327−6330.
39. Holme, E., and Lindstedt, S. (1982) Studies on the partial reaction of thymine 7-hydroxylase in the presence of 5-fluorouracil, *Biochim. Biophys. Acta 704*, 278−283.

40. Myllylä, R., Majamaa, K., Günzler, V., Hanauske-Abel, H. N., and Kivirikko, K. I. (1984) Ascorbate is consumed stoichiometrically in the uncoupled reactions catalyzed by prolyl 4-hydroxylase and lysyl hydroxylase, *J. Biol. Chem. 259*, 5403−5405.
41. Kalliri, E., Grzyska, P. K., and Hausinger, R. P. (2005) Kinetic and spectroscopic investigation of Co^{II}, Ni^{II}, and *N*-oxalylglycine inhibition of the Fe^{II}/α-ketoglutarate dioxygenase, TauD, *Biochem. Biophys. Res. Commun. 338*, 191−197.
42. Baader, E., Tschank, G., Baringhaus, K. H., Burghard, H., and Gunzler, V. (1994) Inhibition of prolyl 4-hydroxylase by oxalyl amino acid derivatives in vitro, in isolated microsomes and in embryonic chicken tissues, *Biochem. J. 300*, 525−530.
43. Cunliffe, C. J., Franklin, T. J., Hales, N. J., and Hill, G. B. (1992) Novel inhibitors of prolyl 4-hydroxylase. 3. Inhibition by the substrate analogue N-oxaloglycine and its derivatives, *J. Med. Chem. 35*, 2652−2658.
44. Chan, D. A., Sutphin, P. D., Denko, N. C., and Giaccia, A. J. (2002) Role of prolyl hydroxylation in oncogenically stabilized hypoxia-inducible factor-1a, *J. Biol. Chem. 277*, 40112−40117.
45. McDonough, M. A., McNeill, L. A., Tilliet, M., Papmichaël, C. A., Chen, Q.-Y., Banerji, B., Hewitson, K. S., and Schofield, C. J. (2005) Selective inhibition of factor inhibiting hypoxia-inducible factor, *J. Am. Chem. Soc. 127*, 7680−7681.
46. Elkins, J. M., Ryle, M. J., Clifton, I. J., Dunning Hotopp, J. C., Lloyd, J. S., Burzlaff, N. I., Baldwin, J. E., Hausinger, R. P., and Roach, P. L. (2002) X-ray crystal structure of *Escherichia coli* taurine/α-ketoglutarate dioxygenase complexed to ferrous iron and substrates, *Biochemistry 41*, 5185−5192.
47. Tramontano, A., and Morea, V. (2003) Assessment of homology-based predictions in CASP5, *Proteins: Struct., Funct., Genet. 53*, 352−368.
48. Kryshtafovych, A., Venclovas, C., Fidelis, K., and Moult, J. (2005) Progress over the first decade of CASP experiments, *Proteins: Struct., Funct., Genet. S7*, 225−236.
49. Clifton, I. J., McDonough, M. A., Ehrismann, D., Kershaw, N. J., Granatino, N., and Schofield, C. J. (2006) Structural studies on 2-oxoglutarate oxygenases and related double-stranded *β*-helix fold protein, *J. Inorg. Biochem. 100*, 644−669.
50. Muller, M., and Moller, K. M. (1969) Urate oxidase and its association with peroxisomes in Acanthamoeba sp., *Eur. J. Biochem. 9*, 424−430.
51. Leighton, F., Poole, B., Lazarow, P. B., and de Duve, C. (1969) The synthesis and turnover of rat liver peroxisomes. I. Fractionation of peroxisome proteins, *J. Cell. Biochem. 41*, 521−535.
52. Nguyen, T., Zelechowska, M., Foster, V., Bergmann, H., and Verma, D. P. S. (1985) Primary structure of the soybean nodulin-35 gene encoding uricase II localized in the peroxisomes of uninfected cells of nodules, *Proc. Natl. Acad. Sci. U.S.A. 82*, 5040−5044.
53. Breidenbach, R. W., Kahn, A., and Beevers, H. (1968) Characterization of glyoxysomes from castor bean endosperm, *Plant Physiol. 43*, 705−713.
54. de Hoop, M. J., and Ab, G. (1992) Import of proteins into peroxisomes and other microbodies, *Biochem. J. 286*, 657−669.
55. Petriv, O. I., Tang, L., Titorenko, V. I., and Rachubinski, R. A. (2004) A new definition for the consensus sequence of the peroxisome targeting signal type 2, *J. Mol. Biol. 341*, 119−134.
56. Reumann, S. (2004) Specification of the peroxisome targeting signals type 1 and type 2 of plant peroxisomes by bioinformatics analyses, *Plant Physiol. 135*, 783−800.
57. Swinkels, B. W., Gould, S. J., Bodnar, A. G., Rachubinski, R. A., and Subramaniam, S. (1991) A novel, cleavable peroxisomal targeting signal at the amino-terminus of rat 3-ketoacyl-CoA thiolase, *EMBO J. 10*, 3255−3262.
58. Lee, J. G., Lee, Y. J., Lee, C. H., and Maeng, P. J. (2006) Mutational and functional analysis of the cryptic N-terminal targeting signal for both mitochondria and peroxisomes in yeast peroxisomal citrate synthase, *Biochem 140*, 121−133.
59. Kato, A., Hayashi, M., Kondo, M., and Nishimura, M. (2000) Transport of peroxisomal proteins synthesized as large precursors in plants, *Cell Biochem. Biophys. 32*, 269−275.
60. Julenius, K., Molgaard, A., Gupta, R., and Brunak, S. (2005) Prediction, conservation analysis and structural characterization of mammalian mucin-type O-glycosylation sites, *Glycobiology 15*, 153−164.
61. Blom, N., Gammeltoft, S., and Brunak, S. (1999) Sequence- and structure-based prediction of eukaryotic protein phosphorylation sites, *J. Mol. Biol. 295*, 1351−1362.
62. Cortay, J.-C., Rieul, C., Duclos, B., and Cozzone, A. J. (1986) Characterization of the phosphoproteins of *Escherichia coli* cells by electrophoretic analysis, *Eur. J. Biochem. 159*, 227−237.
63. Ryle, M. J., Padmakumar, R., and Hausinger, R. P. (1999) Stopped-flow kinetic analysis of *Escherichia coli* taurine/α-ketoglutarate dioxygenase: Interactions with α-ketoglutarate, taurine, and oxygen, *Biochemistry 38*, 15278−15286.
64. Fukumori, F., and Hausinger, R. P. (1993) Purification and characterization of 2,4-dichlorophenoxyacetate/α-ketoglutarate dioxygenase, *J. Biol. Chem. 268*, 24311−24317.
65. Mishina, Y., Chen, L. X., and He, C. (2004) Preparation and characterization of the native iron(II)-containing DNA repair AlkB protein directly from *Escherichia coli*, *J. Am. Chem. Soc. 126*, 16930−16936.
66. Vaillancourt, F. H., Yin, J., and Walsh, C. T. (2005) SyrB2 in syringomycin E biosynthesis is a nonheme Fe^{II} α-ketoglutarate- and O_2-dependent halogenase, *Proc. Natl. Acad. Sci. U.S.A. 102*, 10111−10116.
67. Price, J. C., Barr, E. W., Glass, T. E., Krebs, C., and Bollinger, J. M., Jr. (2003) Evidence for hydrogen abstraction from C1 of taurine by the high-spin Fe(IV) intermediate detected during oxygen activation by taurine:α-ketoglutarate dioxygenase (TauD), *J. Am. Chem. Soc. 125*, 13008−13009.
68. Hoffart, L. M., Barr, E. W., Guyer, R. B., Bollinger, J. M., Jr., and Krebs, C. (2006) Direct spectroscopic detection of a C-H-cleaving high-spin Fe(IV) complex in a prolyl-4-hydroxylase, *Proc. Natl. Acad. Sci. U.S.A. 103*, 14738−14743.
69. Busby, R. W., Chang, M. D.-T., Busby, R. C., Wimp, J., and Townsend, C. A. (1995) Expression and purification of two isozymes of clavaminate synthase and initial characterization of the iron binding site. General error analysis in polymerase chain reaction amplification, *J. Biol. Chem. 270*, 4262−4269.
70. Hegg, E. L., Whiting, A. K., Saari, R. E., McCracken, J., Hausinger, R. P., and Que, L., Jr. (1999) Herbicide-degrading α-keto acid-dependent enzyme TfdA: Metal coordination environment and mechanistic insights, *Biochemistry 38*, 16714−16726.
71. Müller, T. A., Fleischmann, T., van der Meer, J. R., and Kohler, H.-P. E. (2006) Purification and characterization of two enantioselective α-ketoglutarate-dependent dioxygenases, RdpA and SdpA, from *Sphingomonas herbicidovorans* MH, *Appl. Environ. Microbiol. 72*, 4853−4861.
72. Kahnert, A., and Kertesz, M. A. (2000) Characterization of a sulfur-regulated oxygenative alkylsulfatase from *Pseudomonas putida* S-313, *J. Biol. Chem. 275*, 31661−31667.
73. Elion, G. B., Kovensky, A., and Hitchings, G. H. (1966) Metabolic studies of allopurinol, an inhibitor of xanthine oxidase, *Biochem. Pharmacol. 15*, 863−880.
74. Edmondson, D., Ballou, D. P., Van Heuvelen, A., Palmer, G., and Massey, V. (1973) Kinetic studies on the substrate reduction of xanthine oxidase, *J. Biol. Chem. 248*, 6135−6144.
75. McWhirter, R. B., and Hille, R. (1991) The reductive half-reaction of xanthine oxidase. Identification of spectral intermediates in the hydroxylation of 2-hydroxy-6-methylpurine, *J. Biol. Chem. 266*, 23724−23731.
76. Ivan, M., Kondo, K., Yang, H., Kim, W., Valiando, J., Ohh, M., Salic, A., Asara, J. M., Lane, W. S., and Kaelin, W. G., Jr. (2001) HIFa targeted for VHL-mediated destruction by proline hydroxylation: Implications for O_2 sensing, *Science 292*, 464−467.
77. Jaakkola, P., Mole, D. R., Tian, Y.-M., Wilson, M. I., Gielbert, J., Gaskell, S. J., von Kriegsheim, A., Hebestreit, H. F., Mukherji, M., Schofield, C. J., Maxwell, P. H., Pugh, C. W., and Ratcliffe, P. J. (2001) Targeting of HIF-a to the von Hippel-Lindau ubiquitylation complex by O_2-regulated prolyl hydroxylation, *Science 292*, 468−472.
78. Hogan, D. A., Auchtung, T. A., and Hausinger, R. P. (1999) Cloning and characterization of a sulfonate/α-ketoglutarate dioxygenase from *Saccharomyces cerevisiae*, *J. Bacteriol. 181*, 5876−5879.
79. Okamoto, K., Matsumoto, K., Hille, R., Eger, B. T., Pai, E. F., and Nishino, T. (2004) The crystal structure of xanthine oxidoreductase during catalysis: Implications for reaction mechanism and enzyme inhibition, *Proc. Natl. Acad. Sci. U.S.A. 101*, 7931−7936.
80. Retailleau, P., Colloc'h, N., Vivarés, D., Bonneté, F., Castro, B., El Hajji, M., Mornon, J.-P., Monard, G., and Prangé, T. (2004) Complexed and ligand-free high-resolution structures of urate oxidase (Uox) from *Aspergillus flavus*: A reassignment of the active-site binding mode, *Acta Crystallogr. D60*, 453−462.

BI700065H